Towards nanoimprint lithography-aware layout design checking

Citation: Taylor, Hayden, and Duane Boning. "Towards nanoimprint lithography-aware layout design checking." Design for Manufacturability through Design-Process Integration IV. Ed. Michael L. Rieger & Joerg Thiele. San Jose, California, USA: SPIE, 2010. 76410U-12. ©2010 SPIE.

As Published: http://dx.doi.org/10.1117/12.846499

Publisher: SPIE

Persistent URL: http://hdl.handle.net/1721.1/58569

Version: Final published version: final published article, as it appeared in a journal, conference proceedings, or other formally published context

Towards nanoimprint lithography-aware layout design checking

Hayden Taylor*, Duane Boning
Microsystems Technology Laboratories, Massachusetts Institute of Technology
Room 39-328, 77 Massachusetts Avenue, Cambridge, MA USA 02139

ABSTRACT

Just as the simulation of photolithography has enabled resolution-enhancement through Optical Proximity Correction, the physical simulation of nanoimprint lithography is needed to guide the design of products that will use this process. We present an extremely fast method for simulating thermal nanoimprint lithography. The technique encapsulates the resist's mechanical behavior using an analytical function for its surface deformation when loaded at a single location. It takes a discretized stamp design and finds resist and stamp deflections in a series of steps. We further accelerate the simulation of feature-rich patterns by pre-computing dimensionless relationships between the applied pressure, the resist's mechanical properties, and the residual layer thickness, for stamps patterned with uniform arrays of a variety of common feature shapes. The approach is fast enough to be used iteratively when selecting processing parameters and refining layouts. The approach is demonstrated in action with three nanoimprint test-patterns, and describes experimentally measured residual layer thickness variations to within 10–15% or better. Finally, our technique is used to propose nanoimprint-aware design rules.

Keywords: nanoimprint lithography, simulation, design rules, pattern dependencies, computer-aided design, design-for-manufacture

1. INTRODUCTION

As the applications of nanoimprint lithography (NIL) expand, its industrial users are acknowledging a need to model and control the strong, systematic pattern dependencies that are inherent in the process. In this paper we focus on thermal nanoimprint lithography, in which a spun-on thermoplastic resist is softened with heat, imprinted with a relatively hard, wafer-sized stamp, and then cooled to solidify the pattern formed. In thermal NIL, stamps with large or very varied feature sizes, or with large spatial variation of the features' areal densities, experience elastic deflections during imprinting. These deflections cause non-uniformity of the polymeric layer's residual thickness[1-3], which can result in damaging critical-dimension variation (Figure 1). Moreover, problematic stamps take longer to imprint and may never achieve complete replication in the polymer.

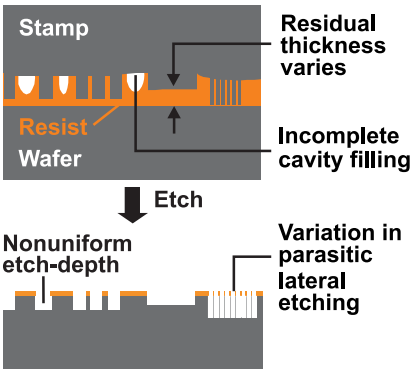

Figure 1. Illustration of parasitic pattern-dependent variations in thermal nanoimprint lithography. Incomplete cavity filling can lead to through-etching of the resist mask in unwanted locations. Meanwhile, residual layer-thickness variation can result in spatially nonuniform vertical etch depths and consequently in variation of lateral critical dimensions.

* hkt@alum.mit.edu; phone 1 617 253-0075

Design for Manufacturability through Design-Process Integration IV, edited by Michael L. Rieger, Joerg Thiele,
Proc. of SPIE Vol. 7641, 76410U · © 2010 SPIE · CCC code: 0277-786X/10/$18 · doi: 10.1117/12.846499

1.1 Tackling pattern dependencies in nanoimprint lithography

Broadly speaking, regions of a stamp with few cavities or large protrusions require higher stamp–resist contact pressures for imprinting, and relatively thick residual layers are observed if such regions are combined on a stamp with regions of smaller protrusions[4]. Attempts to avoid these pattern dependencies have included introducing dummy features to a stamp to homogenize pattern density, although it is recognized that in many devices there is limited freedom to vary the layout[5].

Hybrids of photolithography and mechanical imprinting have been proposed, in order to eliminate the residual layer[6,7] or to circumvent the problems of non-uniform pattern distribution by forming fine features with imprinting and large features with photolithography, so that extensive lateral displacement of material via squeezing is not needed. 'Hybrid' processes, of course, require more fabrication steps and presumably therefore involve greater cost than a simple, single imprint step.

One consequence of pattern density nonuniformity is that it may be impossible to select an initial layer thickness for spun-on resist that is suitable for every region of a stamp. Regions with few cavities will end up with a local surplus of material and large residual layers; meanwhile regions with few protrusions and large cavities will be incompletely filled. Incomplete filling could be problematic in two ways. Firstly, if the imprinted pattern is to form part of a functional structure, incomplete filling is likely to be unacceptable. If, however, the aim of imprinting is to produce an etch-mask, incomplete filling might not in itself be disastrous. The only requirement is that the resist in non-residual regions be thick enough to withstand the whole etching process. The danger here, though, is that if the viscosity of the resist is too low during imprinting then 'capillary bridges' of resist can be formed between the wafer and the top of the unfilled cavity[8]. The action of the resist's surface tension can 'suck' resist away from the wafer such that parts of the resist that are supposed to be thick and to mask the wafer become too thin to be effective as an etch mask.

It appears, then, that there is no easy solution to the dual challenges of incomplete cavity filling and residual layer nonuniformity. Efficient numerical simulation of the imprinting of complete stamp patterns, though, could provide the insights that engineers need to refine designs and select appropriate processing parameters. Given the wide range of possible applications of imprinting/embossing processes and the corresponding variety of lateral feature sizes and imprinted polymer layer thicknesses, it seems that what is needed is a simulation approach that can describe in a unified way the imprinting of features that are wider than, comparable to, and narrower than the thickness of the imprinted polymer layer.

Just as the simulation of photolithography has enabled optical proximity correction (OPC) techniques to enter use, and just as the physical modeling of chemical–mechanical polishing has informed metal layout rules, the physical simulation of nanoimprint lithography is needed to guide the design of products that will be amenable to manufacturing using this process. Nanoimprint-aware design checks should be able to assess whether a given pattern can be fully imprinted in an acceptable time, and whether any parasitic residual layer of imprinted resist is sufficiently thin and uniform. Nanoimprint simulation could be used:

- At the very end of the design process, when the layout has been fixed, to select appropriate nanoimprint process parameters. It is likely, though, that the process parameters will be fixed for a given fabrication facility, so that the *design* will need to conform to certain specifications;
- Between stamp design and fabrication, as part of an automatic software tool that would systematically modify the shapes of individual stamp features. Any modifications would aim to make the design more amenable to replication with NIL. This procedure would be analogous to Optical Proximity Correction for photolithography;
- At the chip-level, at the very end of the design process, to provide model-based checking of manufacturability. The software would highlight any locations on the chip that would be defect-prone during imprinting. At this stage, if problems were found, manual layout changes by engineers would still be possible;
- At the cell- or block-level, to provide model-based design checking as an integral part of the design process. It would be normal for the design check to be run several times — even, perhaps, five or ten times in a day — as a designer refined their layout;
- To create a set of nanoimprint-aware 'design-rules' that would be incorporated into existing design-rule checks.

These possible modes of use suggest that there may well be a need to run cell- or block-level design checks (containing hundreds to millions of features) within a fraction of a working day. Engineers working on a specific layout block cannot necessarily command the use of a processor farm to make these frequent design checks, and might well need to be able to run the checks using their own workstations. What is needed, therefore, is a highly computationally efficient simulation approach.

1.2 Existing nanoimprint simulation approaches

There is a large body of experimental work in the literature that describes pattern dependencies in nanoimprint lithography. Much of this work attempts to explain the observed phenomena through numerical simulation. The simulations reported are generally for a single feature and assume plane-strain geometry. There have been far fewer attempts to simulate the embossing of feature-rich patterns.

Finite-element approaches. There have been several attempts to describe thermal nanoimprint lithography through the finite-element modeling of very simple geometries[9-13]. The embossed material layer has variously been described as a Newtonian liquid[9-11,14], as a shear-thinning liquid[9], and with linear viscoelastic[12,15] models. Surface tension effects have generally been regarded as negligible in the simulation of thermoplastic NIL, where the polymer's viscosity during imprinting is usually at least 10^3 Pa.s and bulk forces are considered to dominate over surface forces. Indeed, of the feature-scale, thermal NIL simulation work surveyed, only the work of Jeong accounts for capillary force effects[14]. Finite-element approaches certainly capture many of the physical phenomena observed in nanoimprint. They are currently too computationally costly, though, to extend to the feature-rich patterns of complete devices.

'Coarse-grain' approaches. For the simulation of thermal nanoimprint lithography, Zaitsev *et al.* have proposed a simplified 'coarse-grain' approach in which the imprinted polymeric layer is modeled as a Newtonian fluid and the pattern of the stamp is represented by a matrix of cells, each assumed to contain features of a single size and packing density[4,16]. The solution procedure assumes an elastic model for the deflections of the stamp and the substrate and confines motion of the Newtonian resist to being parallel to the plane of the substrate. Simplified Navier-Stokes equations are solved assuming a constant stamp velocity. Simulation durations are reported to be in the region of 20 minutes for a 128-square grid of cells[16]. To produce a simulation tool that could be used iteratively in the design process — with simulations perhaps needing to be run by an engineer several times each day — a further substantial increase in simulation speed would be beneficial.

Contact mechanics-based approaches. Efficient numerical simulations of the deformations of elastic and elastic-plastic bodies[17,18] have been widely used by researchers in tribology. These simulations rely on a description of the deformation of the material's surface in response to a point-load, together with, in the elastic-plastic cases, a criterion for yielding of the material. The overall topography of the material's surface is calculated by spatially convolving an iteratively-found contact pressure distribution with the point-load response. Sub-surface stresses can similarly be estimated by convolving contact pressures with the appropriate kernel functions[17]. The convolution itself can be effected using fast Fourier transforms[18,19] or other summation methods. The solution for the contact-pressure distribution has successfully been performed with iterative conjugate-gradient methods combined with kinematic constraints on the surface deformation, or with methods that seek a minimum of elastic potential energy in the layer.

1.3 The proposed new simulation approach

In our earlier work[20], we built upon the contact mechanics-based approaches described above to provide a way of simulating the micron-scale embossing of millimeter-thickness thermoplastic polymers for microfluidic applications. We later extended this approach to model the embossing of thermoplastic films that were as little as a few micrometers thick[21], provided that the total depth of embossing was a small proportion of the original film thickness. Here, we extend the technique further and present an extremely fast method for simulating the thermal nanoimprint process. We capture elastic stamp deflections and can describe the formation of arbitrarily thin residual layers. Our method offers yet faster simulation speeds than demonstrated by others, and the capability to model linear viscoelastic resists as well as simply Newtonian ones.

2. MODELING APPROACH

2.1 Modeling resist deformation

We encapsulate the resist's mechanical behavior using an analytical function for its surface deformation when loaded at a single location (Figure 2b). Both O'Sullivan and King[22] and Nogi and Kato[18] make use of an expression for the surface deformation of a linear-elastic layer of finite thickness on an elastic substrate, when exposed to unit normal pressure across a small square region of its surface. We adapt this expression for the imprinting of a linear *visco*elastic layer on a hard substrate as follows. We observe that the imprinting of a linear viscoelastic layer with time-evolving compliance $J(t)$ and exposed to a stamp-average pressure $p_0(t)$ produces the same topography at time t as does the imprinting of a 'virtual', *purely elastic* layer having a dimensionless elastic modulus of $(1–\nu^2)$ and loaded instantaneously with the dimensionless, spatial-average pressure quantity $p_{g,0}$:

$$p_{g,0}(t) = (1-\nu^2)\int_0^t \frac{1}{D^2}\int_0^D\int_0^D p(x,y,t')\,\mathrm{d}x\mathrm{d}y\,\frac{\mathrm{d}J(t-t')}{\mathrm{d}t'}\mathrm{d}t' = (1-\nu^2)\int_0^t p_0(t')\frac{\mathrm{d}J(t-t')}{\mathrm{d}t'}\mathrm{d}t'. \quad (1)$$

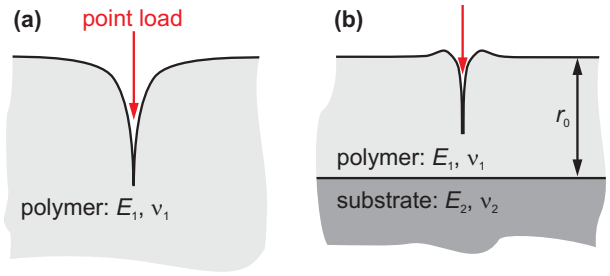

Figure 2. Illustration of the point-load responses of polymeric layers. In our earlier work addressing the micro-embossing of thick polymeric plates[20], the response of the surface topography to loading at a single location took the form shown in (a). Meanwhile, in thermal nanoimprint — where the layer thickness is comparable with the lateral discretization pitch of the simulation — a different function shape is required, to represent the lateral transport of resist material (b). For a viscoelastic material, the point-load response is a function of time as well as of position.

We believe that a linear viscoelastic resist model provides a reasonable and conservative estimate of residual layer thicknesses and the extent of cavity filling. Shear-thinning, while observed with some thermal nanoimprint resists and especially noticeable when imprinted features have widths of many micrometers, would be expected to lead to thinner residual layers and more complete filling than a linear model predicts. A Newtonian (purely viscous) resist model may well suffice for imprinting conditions that are sufficiently far above the resist's glass-transition temperature. For a Newtonian resist, the compliance function is $J(t) = t/\eta$, where η is the viscosity of the resist at the temperature of imprinting.

For an arbitrarily patterned stamp, then, the simulation procedure for a uniform incremental change $–\Delta r$ in residual layer thickness involves finding the virtual contact pressure distribution $\Delta p_g(x, y)$ that, when convolved in space with the point-load response $g(x,y)$ of the virtual elastic polymer, yields the incremental residual layer thickness reduction. In our implementation, the solution is found with a biconjugate gradient method. For imprinting processes where the residual layer is reduced to a small proportion of its original thickness r_0, the simulation needs to be performed in a series of steps, with the value of $g(x,y)$ being re-evaluated at each step to account for the reducing layer thickness, and with the evolving shape of the stamp–resist contact region C being tracked. When cavities of a stamp begin to be filled, the layer thickness inside the contact region will vary with position, and if the stamp has only one value of cavity height, h, we can write the convolution for an incremental layer-thickness reduction by using one point-load response, g_{top}, for the tops of the cavities (where the layer thickness is $r+h$) and another, g_{bottom}, for the residual-layer regions (where the layer thickness is r). The simulations are performed in discrete space with lateral pitch d, so that $x_m = dm$ and $y_n = dn$:

$$\left(\Delta p_g[m,n]k_{bottom}[m,n]\right) * g_{bottom}[m,n] + \left(\Delta p_g[m,n]k_{top}[m,n]\right) * g_{top}[m,n] = -\Delta r \qquad \forall\, m,n \in C. \quad (2)$$

The function $k_{top}[m, n]$ is set to 1 inside cavity regions and zero outside, and $k_{bottom}[m, n] = 1 - k_{top}[m, n]$. $\Delta p_g[m, n]$ is zero outside C. Through such a stepping procedure, relationships between p_g and r can be built up for any given pattern.

2.2 Abstracting the imprinting of feature-rich patterns

We further accelerate the simulation of feature-rich patterns in the following way. We pre-compute relationships between the applied pressure–compliance integral $p_{g,0}(t)$ and the residual layer thickness (Figure 3), for stamps patterned with uniform arrays of a variety of common feature shapes. These relationships are encoded in a dimensionless form: we define a dimensionless residual layer thickness $r' = r/a$, where a is a characteristic stamp protrusion diameter for the pattern.

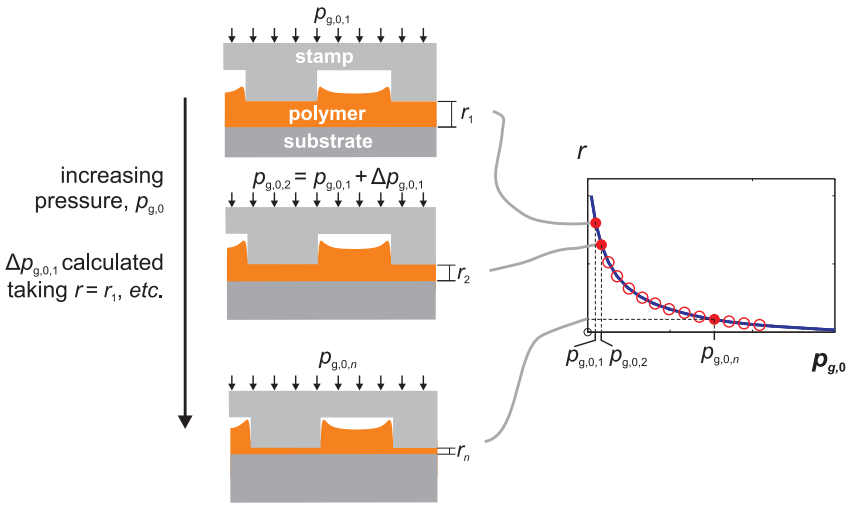

Figure 3. Residual layer thickness-stepping method for determining the relationship between the applied pressure–compliance integral $p_{g,0}$ and residual thickness r.

For the case where cavities are tall enough that they never completely fill, the following cubic equation has been found to describe well the relationship between the differential pressure–compliance needed and the dimensionless residual layer thickness: F_1 is a dimensionless pattern-dependent constant that dominates when $r' << 1$, F_3 dominates for thick polymeric layers, and F_2 captures the important transition region when $r' \approx 1$. These F-constants have been determined, and where appropriate fit as polynomial functions of pattern density, for stamps carrying uniform arrays of parallel ridges, square holes, and circular protrusions.

$$-\frac{\mathrm{d}p_{g,0}}{\rho\,\mathrm{d}r'} = F_1(r')^{-3} + F_2(r')^{-2} + F_3 \cdot \tag{3}$$

In Figure 4a are shown, for arrays of parallel lines with four values of areal protrusion density ρ, the relationships between $\mathrm{d}p_{g,0}/\mathrm{d}r'$ and r'. The heavy dashed line indicates the results of numerical, stepped simulations as illustrated in Figure 3, while the solid lines show the model fit according to Equation (3). The integration of this function with respect to r' enables a $p_{g,0}$–r' relationship for residual layer squeezing to be plotted, as in Figure 4b.

If, however, as is more usual, the cavities are shallow enough that they are able to fill with resist, the residual layer thickness has a lower limit that must be represented. We have found that a reasonable approximation to the $p_{g,0}$–r' relationship during filling can be obtained using an exponential function that asymptotically approaches a limiting minimum of r' for large $p_{g,0}$ and completely filled cavities. The overall $p_{g,0}$–r' relationship, taking into account both residual layer squeezing and cavity filling, is represented by taking the maximum of the r' values corresponding to the two phenomena. Full details of the relevant functions will be presented in a future publication.

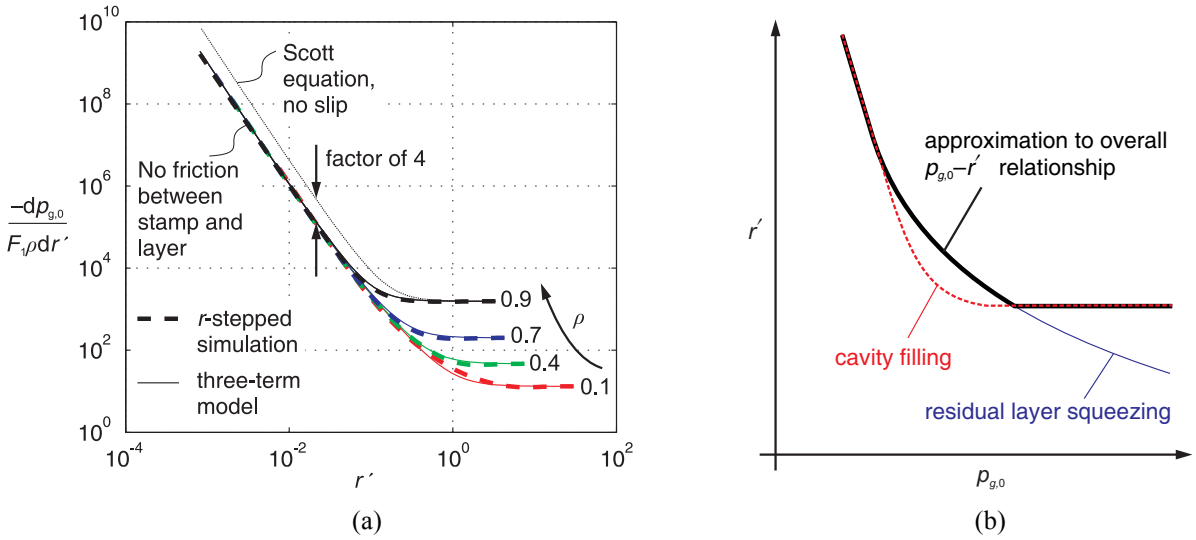

Figure 4. (a) Relationship between $dp_{g,0}/\rho dr'$ and r' for embossing with a stamp having an infinitely large array of parallel lines and trenches. (b) Schematic illustrating the approximation that captures the effect of cavity filling on the relationship between $p_{g,0}$ and r'.

2.3 Modeling stamp deflections

The stamp and substrate, meanwhile, are well modeled as linear-elastic and we distinguish between local stamp/substrate *indentation* and stamp *bending*, which dominates when the spatial period of the pattern is more than about four times the stamp thickness. Stamp deflections are computed by convolving the stamp–resist contact pressure distribution with the sum of two kernel functions: one describing the point-load response of an elastic half-space of stamp material (for the indentation mode), and the other describing the bending of one square period of a plate with infinitely large lateral extent, loaded on one side with a square array of point forces and on the other with a balancing uniform pressure. This second, bending, kernel function could be obtained analytically using small-deflection plate theory, or through finite-element simulation, or by applying the formulae of Nogi and Kato[18] for the deformation of a finite-thickness elastic layer, assuming the underlying substrate to be much less stiff than the stamp layer.

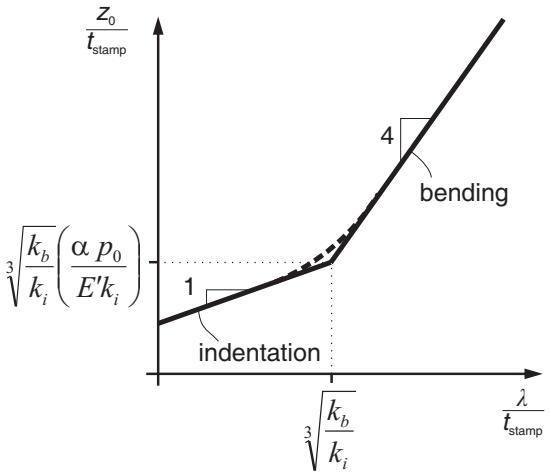

Figure 5. Schematic graph, on logarithmic axes, of the maximum surface waviness z_0 to which a stamp can conform, as a function of the applied average pressure, p_0, the maximum allowable pressure nonuniformity α (defined as a proportion of p_0), the stamp material's plate modulus E', and the characteristic wavelength, λ, of surface roughness. Bending dominates over indentation when λ divided by the stamp thickness, t_{stamp}, exceeds $(k_b/k_i)^{1/3} \approx 4$.

2.4 Modeling the complete nanoimprint process

We now bring together the models for polymer layer deformation and stamp/substrate deflections to construct a die-scale, hierarchical simulation method. As shown in Figure 6, each (identical) $D \times D$ die on the stamp is discretized into regions of size $d \times d$. The die design is described by a 'coarse' topography $w_{stamp}[m, n]$ that takes a uniform value within any given $d \times d$ region, upon which is superimposed a 'fine' topography characterized within each $d \times d$ region by a homogeneous, regular pattern of a particular pitch, shape, and areal density. In this way, we can use a single simulation approach both for large, feature-rich patterns and for intricate custom patterns discretized at the sub-feature scale.

Our approach takes this discretized stamp design and finds resist and stamp deflections in a series of steps. The compliance of the resist is gradually increased with each step, and the algorithm iteratively finds the distribution of stamp–resist contact pressure that is consistent with the instantaneous compliances of the stamp and resist. At each step, the sum of the coarse stamp topography, plus stamp, substrate, and resist deformations at each location must sum to a spatially uniform reference displacement, Δ:

$$w_{stamp}[m,n]+w_{D,die}[m,n]+w_{D,substrate}[m,n]+w_{local}[m,n]+w_{die}[m,n]=\Delta \qquad \forall\ m,n \in C \tag{4}$$

$w_{D,die}$ are the elastic stamp deflections, $w_{D,substrate}$ are the elastic deflections of the underlying wafer (assumed thick and rigidly supported), $w_{local}[m,n]$ is the movement of the stamp associated with the forcing of resist into cavities inside the region $[m,n]$, and $w_{die}[m,n]$ is the movement of the stamp associated with lateral displacement of resist between differently patterned local regions of the stamp. Typically resist will be displaced out of regions with a small cavity density and into adjacent regions with more or larger cavities.

Incremental changes in resist layer thicknesses are computed at each step by convolving the found pressure distribution with an appropriately scaled version of the resist's point-load response, at a spatial discretization pitch of d. The p_g–r gradient associated with the local filling of each $d \times d$ region must also be computed, and contributes to the incremental stamp displacements. After each step, the minimum resist layer thickness in each $d \times d$ region is re-evaluated and the system is re-linearized for the next step. At the final step, the modeled compliance of the resist is consistent with that at the end of the imprinting cycle, and the distribution of the resist's residual layer thickness is reported.

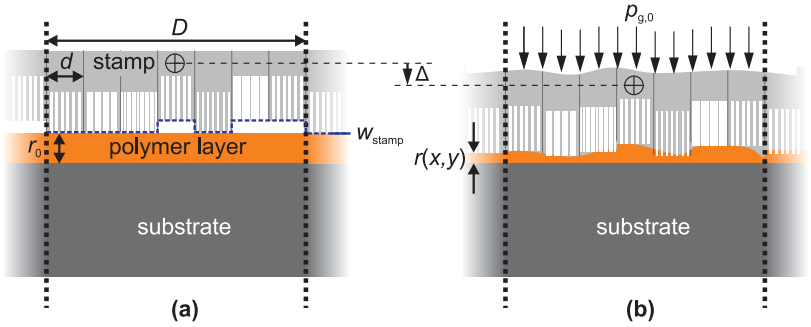

Figure 6. Outline of chip-scale simulation approach for thermal nanoimprint. The wafer is assumed to be arrayed with identical chips of size $D \times D$. The chip design is subdivided into regions of diameter d, each characterized by a particular feature shape, size, and packing density. Stamp and polymer deflections are illustrated: (a) before any imprinting pressure is applied; (b) at the end of the imprinting process. The external imprinting load is modeled as being applied hydrostatically to the back-side of the stamp. Not to scale.

3. EXPERIMENTAL METHOD

As a demonstration of the simulation method, we now compare experimental results from the imprinting of two simple test patterns with the results of simulations assuming a Newtonian resist model. Silicon stamps carrying the test patterns were etched to a depth of approximately 30 μm using deep reactive ion etching. This relatively large etch-depth was chosen so that none of the stamp cavities would fill during imprinting. The first test pattern incorporates a set of square and L-shaped protrusions varying in diameter from 5 to 50 μm. The pattern was tiled on the wafer in a large square array with a lateral period of 425 μm. The second test pattern comprises an 8×8 patchwork of regions, each

region of the stamp containing either parallel lines or square holes with pitches ranging from 25 to 100 μm and areal protrusion densities ranging from 10 to 90%. This second pattern has a diameter of 4 mm and was tiled across the wafer as a square array.

A die-saw was used to cut a 10 mm-pitch square grid of *c*. 150 μm-wide, *c*. 400 μm-deep grooves into the unpolished backside of a 625 μm-thickness silicon wafer piece. The wafer piece was then cleaned with acetone and methanol, and dried in a nitrogen stream. The polished side of the silicon was spin-coated at 3000 rpm for 1 minute with 495 kg/mol polymethylmethacrylate (PMMA) dissolved 3% by weight in anisole. The coated piece was heated to 180 °C for one minute on a hot-plate, and then fractured into 10 mm square pieces by making use of the backside grooves. Taking this approach — rather than spin-coating individual 10 mm-square pieces — avoided the presence of edge-beads of resist on the samples. The thickness of the PMMA coating was determined by stylus profilometry to be 200±10 nm.

The samples were then imprinted using either a modified Instron materials-testing machine (in the case of the first pattern) or a custom-made, pneumatically-actuated imprinting system[23] (in the case of the second pattern). Both machines had electrically heated aluminum platens. The first test pattern (with L-shaped protrusions) was imprinted at 165±5 °C, under a 40 MPa sample-average applied pressure. The load was held for one minute before the temperature started to be reduced; the temperature then took approximately one further minute to fall to approximately 70 °C, at which time the load was removed. The second test pattern (with the richer patchwork of features) was imprinted at 170±5 °C under a sample-average pressure between 10 and 15 MPa, for durations of between 1 and 5 minutes. In each case, once the loading duration had elapsed the platens took approximately one further minute to cool to an unloading temperature below PMMA's glass-transition of approximately 105 °C. After imprinting, the samples were sputtered with approximately 100 nm of gold and profiled in a scanning white-light interferometer.

4. RESULTS AND DISCUSSION

4.1 Feature-level simulation

We first consider the imprinting of the test pattern with L-shaped protrusions. Here, the simulation was performed at the level of individual features, without recourse to the pattern-abstraction methods described above. We assume a Young's modulus for the silicon stamp and substrate of 160 GPa and a Poisson's ratio of 0.27. We find that the simulation closely matches the experimental data for a resist viscosity of 10^7 Pa.s, which corresponds reasonably well with literature values[24] for the zero-shear viscosity of PMMA at 165 °C. Figure 7 shows that the shape of the simulated residual layer profile agrees reasonably closely with that measured experimentally — both across the whole pattern and within individual features. The experimental data do show sharper central residual layer peaks in the widest features: these peaks are indicative of shear-thinning. The simulation approach described here makes no allowance for shear thinning, and so cannot describe such peaks, but the overall simulation is faithful nevertheless. In any case, stamp protrusion diameters of many tens of microns are unlikely to be particularly prevalent in manufactured devices where the imprinted layer is of sub-micron thickness.

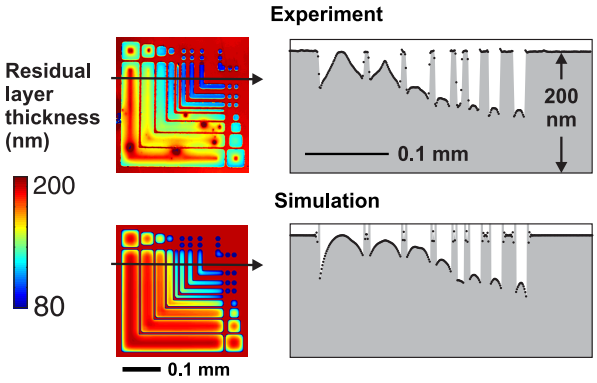

Figure 7. Experimental and simulated topography plots and cross-sections for a test pattern having features ranging from 5 to 50 μm in diameter, imprinted into 495 kg/mol PMMA of 200 nm initial thickness. Imprint conditions were c. 165 °C, 40 MPa average applied pressure, and 1 minute loading duration.

4.2 'Patchwork' test-pattern

We now turn to the imprinting of the 4 mm-period patchwork of features. Here, we employ the pattern-extraction techniques described above, and the design is represented for simulation as a 64×64 array of regions. Based on the modest amount of experimental data available (Figure 8), it appears that the technique can track with some fidelity the evolution of residual layer thickness with time. A resist viscosity of 10^6 Pa.s was assumed for these simulations.

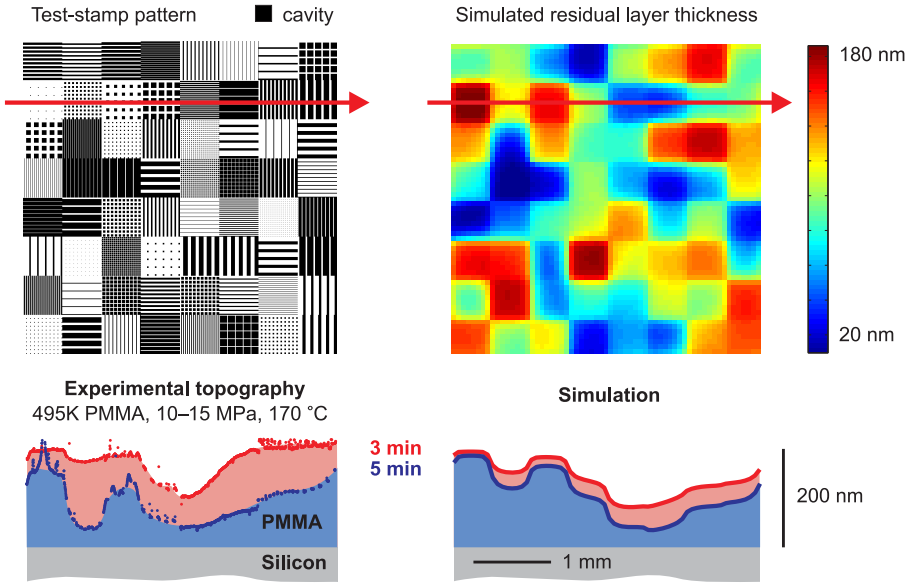

Figure 8. Experimental and simulated topographies for the imprinting of 495 kg/mol PMMA of 200 nm initial thickness. Imprint conditions were c. 170 °C, 10–15 MPa average applied pressure, and 3 and 5 minute loading durations. The cross-sectional topographies plotted at the bottom of the figure correspond to the arrows drawn through the 2-D plots above.

4.3 Comparison with results of Kehagias *et al.*

Finally, we evaluate the ability of our simulation approach to represent the experimental results published by Kehagias et al[4]. In this work, 75 kg/mol PMMA was imprinted with a silicon stamp having rectangular protrusions varying in pitch and diameter, none narrower than 10 µm. We have used our simulation technique in its 'hierarchical' (pattern-abstraction) mode to produce simulations of residual layer thickness, the proportions of cavity-volumes filled, and the stamp–resist contact pressure distribution at the end of the five-minute imprinting cycle (Figure 9). Using a literature value of 2×10^5 Pa.s for the viscosity of the resist at the imprinting temperature of 190 °C, the simulated residual-layer thicknesses are within 10–15% of the measured values reported by Kehagias.

4.4 Time required for simulations

The simulation technique is implemented in Matlab and the convolution steps use fast Fourier transforms. In Figure 10, simulation times for the three patterns shown in this paper are plotted against the number of discrete spatial regions, N, along one side of the simulation space. Simulations were carried out using a personal computer with a 3 GHz Intel Pentium processor and 3 GB RAM. We see that simulations using our method are at least 10^3 times faster than those estimated for feature-level simulations carried out using the finite-element method[20]. An optimized and/or compiled implementation of our approach could offer yet faster simulation speeds. The simulation times that we report are consonant with our envisaged use of simulation at the cell-level, for designs incorporating on the order of several hundred features, to guide iterative refinement of physical layout. We also anticipate being able to develop the technique to provide reasonably fast pre-manufacturing checks of chip-scale designs, including many millions of features.

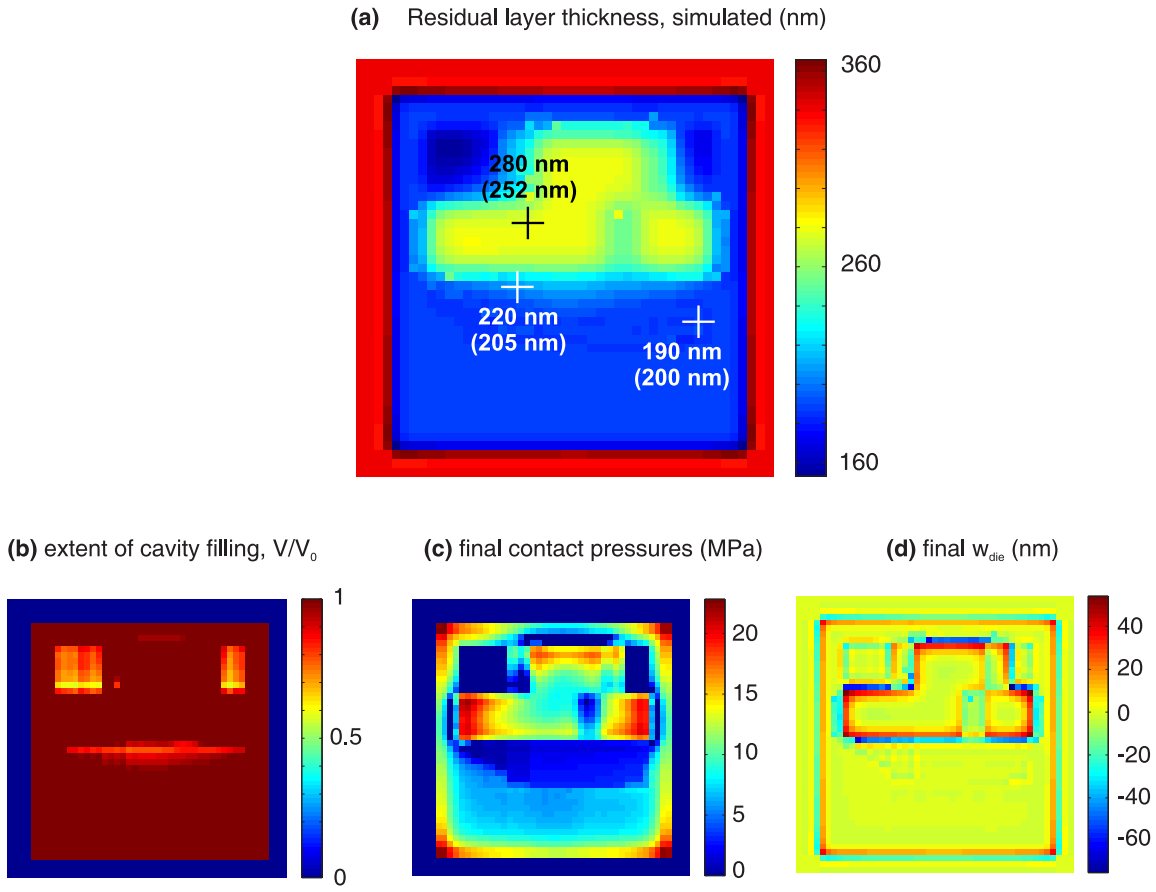

Figure 9. The result of applying our simulation technique to the experimental conditions reported by Kehagias[4]. A 340 nm layer of 75 kg/mol PMMA was imprinted by Kehagias at 190 ˚C under 6 MPa for 5 min. The stamp design has arrays of rectangular cavities of depth 300 nm and with various widths all exceeding 10 μm. Residual layer thicknesses simulated using our fast method are shown in (a). Simulated residual layer thickness values at three particular locations are indicated in numbers, and the corresponding, experimentally measured values reported by Kehagias are shown in parentheses. Simulation and experiment match to within 10–15 %. In (b), the simulated proportion of cavity volume filled is mapped. The contact pressure distribution simulated for the end of the five-minute loading cycle is shown in (c). The net intra-die displacement of material at the end of the imprinting cycle is mapped in (d): displacement *out* of a region is positive.

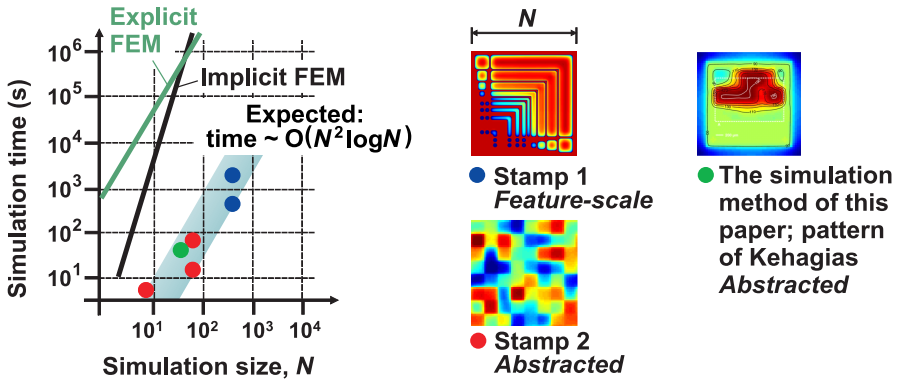

Figure 10. Simulation times for the three stamp patterns described in this paper. The simulation time scales, as expected, roughly as $N^2 \log N$, where N is the number of spatial regions along one side of the two-dimensional imprinted region being simulated.

4.5 Possible design rules

Guidance on feature diameters. Having decided how large a residual layer thickness (RLT) and how much variation of it they can accept, NIL engineers will want to design the stamp and the imprinting process to meet those specifications — usually with as little imprinting time as possible. It can be deduced from Figure 4a that the 'difficulty' of imprinting an array of features into a thin film of resist is proportional to the *square* of the characteristic diameter, a, of stamp protrusions. A sensible design rule would use knowledge of resist properties and imprint machine capabilities to place an upper limit on feature diameters. Designers could be required to insert 'relief' cavities into large protrusions to ease their imprinting.

Guidance on cavity volume density. Around the time when the cavities of a stamp start to become completely filled, most material flow will have been local — over lengths of no more than a single feature diameter — and there will not have been time for much long-range transport of resist material over distances of many feature diameters. Designers would therefore be well advised to distribute the volumes of cavities as uniformly as possible across the stamp. This aim might be achieved through the introduction of dummy cavities or protrusions. The more uniform the residual layer needs to be, the shorter the lateral length scale over which 'uniformity' of cavity volume density should be enforced. If the relief height, h, of the stamp is constant for all features, this design rule is equivalent to requiring the *areal* density of protrusions, ρ, to be uniform.

Guidance on the uniformity of $F_1a^2\rho$. As well as addressing RLT uniformity in cases where cavities are completely filled, it would be valuable to have a design rule for the case where stamp cavities are *not* going to be completely filled. In this situation, the resist layer is 'frozen' when the length-scales of material transport are still comparable to individual feature diameters, and achieving RLT uniformity relies on maintaining uniform stamp and substrate deflections. From Figure 4a, we can see that when residual layers are considerably thinner than the characteristic feature diameter:

$$\frac{\mathrm{d}p_g}{\mathrm{d}r} = F_1 a^2 \rho. \tag{5}$$

Therefore, to keep the local average of stamp–layer contact pressure — and hence stamp/substrate deflections — uniform as r reduces, we require $F_1a^2\rho$ to be kept spatially uniform. As material begins to touch the tops of cavities, or if $a \leq r$, the validity of this design rule is likely to deteriorate, but it does at least provide some guidance.

5. CONCLUSION AND OUTLOOK

We have outlined a fast yet reliable approach to simulating thermal nanoimprint lithography. We have described ways of modeling the deformation of a linear viscoelastic resist as well as the indentation and bending of a relatively hard, elastic stamp. We have also shown a way of abstracting feature-rich patterns, offering a route to the affordable simulation of chip-scale designs. We have demonstrated the simulation technique in action with three different patterns, and have seen that it is capable of capturing pattern-dependent residual layer thickness variations to within 10–15% or better.

The simulation technique has been conceived for the imprinting of spun-on thermoplastic layers, although we anticipate that it can be readily applied to the imprinting of spun-on ultraviolet-curing resists, given an adequate viscosity–time model of the resist. The droplet-dispensing of lower-viscosity, photo-curable imprint resists, meanwhile, is receiving growing interest and it would be valuable to extend this simulation capability for that process. To do so, two major modifications will be required: firstly, the incorporation of capillary forces, and secondly, the capability to model the squeezing and merging of discrete resist droplets between the stamp and substrate.

With fast simulation in place, opportunities open up for automation of NIL-friendly design. We envisage the invention of *mechanical proximity correction* (MPC), in which 'dummy' features would be added to a stamp design and large stamp protrusions would be automatically split and re-shaped to improve a pattern's imprintability. MPC will be a fertile ground for the invention of new algorithms — to the extent of complete systems for turning circuit schematics into manufacturable layout. In a few years MPC could become as pivotal to the use of nanoimprint as optical proximity correction is to the use of photolithography today.

REFERENCES

[1] Scheer, H.-C., Schulz, H., Hoffmann, T. and Sotomayor Torres, C.M., "Problems of the nanoimprinting technique for nanometer scale pattern definition," J. Vac. Sci. Technol. B 16(6), 3917-3921 (1998).

[2] Heyderman, L.J., Schift, H., David, C., Gobrecht, J. and Schweizer, T., "Flow behaviour of thin polymer films used for hot embossing lithography," Microelectronic Engineering 54, 229-245 (2000).

[3] Wissen, M., Schulz, H., Bogdanski, N., Scheer, H.-C., Hirai, Y., Kikuta, H., Ahrens, G., Reuther, F. and Glinsner, T., "Impact of residual layer uniformity on UV stabilization after embossing," J. Vac. Sci. Technol. B 22(6), 3224-3228 (2004).

[4] Kehagias, N., Reboud, V., Sotomayor Torres, C.M. and Sirotkin, V., "Residual layer thickness in nanoimprint: Experiments and coarse-grain simulation," Microelectronic Engineering 85, 846-849 (2008).

[5] Pedersen, R.H., Thamdrup, L.H., Larsen, A.V. and Kristensen, A., "Quantitative Strategies to Handle Stamp Bending in NIL," Proc. Nanoimprint and Nanoprint Technol. (2008).

[6] Guo, L.J., "Recent progress in nanoimprint technology and its applications," *Journal of Physics D: Applied Physics* 37, R123-R141 (2004).

[7] Kehagias, N., Reboud, V., Chansin, G., Zelsmann, M., Jeppesen, C., Schuster, C., Kubenz, M., Reuther, F., Greutzner, G. and Sotomayor Torres, C.M., "Reverse-contact UV nanoimprint lithography for multilayered structure fabrication," Nanotechnology 18(17), 175303 (2007).

[8] Schift, H., Heyderman, L.J., Auf der Maur, M. and Gobrecht, J., "Pattern formation in hot embossing of thin polymer films," Nanotechnology 12(2), 173-177 (2001).

[9] Rowland, H.D., King, W.P., Sun, A.C. and Schunk, P.R., "Impact of polymer film thickness and cavity size on polymer flow during embossing: Toward process design rules for nanoimprint lithography," Journal of Micromechanics and Microengineering 15, 2414-2425 (2005).

[10] Rowland, H.D., King, W.P., Sun, A.C. and Schunk, P.R., "Simulations of nonuniform embossing: The effect of asymmetric neighbor cavities on polymer flow during nanoimprint lithography," J. Vac. Sci. Technol. B 23(6), 2958-2962 (2005).

[11] Young, W.-B., "Analysis of the nanoimprint lithography with a viscous model," Microelectronic Engineering 77(3), 405-411 (2005).

[12] Takagi, H., Takahashi, M., Maeda, R., Onishi, Y., Iriye, Y., Iwasaki, T. and Hirai, Y., "Analysis of time dependent polymer deformation based on a viscoelastic model in thermal imprint process," Microelectronic Engineering 85(5), 902-906 (2008).

[13] Hirai, Y., Konishi, T., Yoshikawa, T. and Yoshida, S., "Simulation and experimental study of polymer deformation in nanoimprint lithography," J. Vac. Sci. Technol. B 22(6) 3288-3293 (2004).

[14] Jeong, J.-H., Choi, Y.-S., Shin, Y.-J., Lee, J.-J., Park, K.-T., Lee, E.-S., Lee, S.-R., "Flow behavior at the embossing stage of nanoimprint lithography," Fibers and Polymers 3, 113-119 (2002).

[15] Hirai, Y., Onishi, Y., Tanabe, T., Shibata, M., Iwasaki, T., Iriye, Y., "Pressure and resist thickness dependency of resist time evolutions profiles in nanoimprint lithography," Microelectronic Engineering 85, 842-845 (2008).

[16] Zaitsev, S., Sirotkin, V., Svintsov, A. and Schift, H., "Coarse-grain method for modeling of stamp and substrate deformation in nanoimprint," Microelectronic Engineering 84, 868-871 (2007).

[17] Johnson, K.L., [Contact Mechanics], Cambridge University Press, Cambridge and New York (1985).

[18] Nogi, T. and Kato, T., "Influence of a hard surface layer on the limit of elastic contact — Part I: Analysis using a real surface model," Journal of Tribology, Transactions of the ASME 119, 493-500 (1997).

[19] Wang, F. and Keer, L.M., "Numerical simulation for three dimensional elastic-plastic contact with hardening behavior," Journal of Tribology, Transactions of the ASME 127, 494-502 (2005).

[20] Taylor, H., Lam, Y.C. and Boning, D., "A computationally simple method for simulating the micro-embossing of thermoplastic layers," Journal of Micromechanics and Microengineering 19, 075007 (2009).

[21] Taylor, H., Iliescu, C., Ni, M., Xing, C., Lam, Y.C. and Boning, D., "Modeling pattern dependencies in the micron-scale embossing of polymeric layers," Proc SPIE 7269, 726909-15 (2008).

[22] O'Sullivan, T.C. and King, R.B., "Sliding contact stress field due to a spherical indenter on a layered elastic half-space," Journal of Tribology, Transactions of the ASME 110, 235-40 (1988).

[23] Hale, M., "Development of a Low-Cost, Rapid-Cycle Hot Embossing System for Microscale Parts," SM thesis, Massachusetts Institute of Technology, Cambridge, MA (2009).

[24] Garcia Romero, I., "Rheological characterisation and tuning of polymers for nanoimprint lithography," Proc. Nanoimprint and Nanoprint Technol. (2008).